Study of optical Tamm states based on the phase properties of one-dimensional photonic crystals

Zefeng Chen,[1,2] Peng Han,[1] Chi Wah Leung,[2] Yu Wang,[2] Mingzhe Hu,[2,3] and Yihang Chen[1,2,*]

[1] *Laboratory of Quantum Information Technology, School of Physics and Telecommunication Engineering, South China Normal University, Guangzhou 510006, China*
[2] *Department of Applied Physics and Materials Research Center, The Hong Kong Polytechnic University, Hong Kong SAR, China*
[3] *College of Science, Guizhou University, Shengdao 101, Huaxi 550025, Guiyang, Guizhou, China*
[*] *yhchen@scnu.edu.cn*

Abstract: We demonstrate the physical mechanism of optical Tamm states using the phase properties of the photonic crystals. Based on such mechanism, we propose an efficient way that can precisely produce optical Tamm states at specific frequencies. Moreover, we show that dielectric photonic crystals and single-negative materials can be effectively connected through their reflection phase. Two kinds of one-dimensional dielectric photonic crystals with different single-negative characteristics are designed and repeated alternately to construct a superlattice structure. The band structures and the transmission spectra of this superlattice show that multiple optical Tamm states arise and these Tamm states are coupled with each other to form transmission bands. A special zero-effective-phase gap can also be observed in such superlattice.

References and links

1. Z. J. He, H. Jia, C. Y. Qiu, S. S. Peng, X. F. Mei, F. Y. Cai, P. Peng, M. Z. Ke, and Z. Y. Liu, "Acoustic transmission enhancement through a periodically structured stiff plate without any opening," Phys. Rev. Lett. **105**(7), 074301 (2010).
2. M. A. Noginov, G. Zhu, M. Mayy, B. A. Ritzo, N. Noginova, and V. A. Podolskiy, "Stimulated emission of surface plasmon polaritons," Phys. Rev. Lett. **101**(22), 226806 (2008).
3. X. S. Wang, A. Bezryadina, Z. G. Chen, K. G. Makris, D. N. Christodoulides, and G. I. Stegeman, "Observation of two-dimensional surface solitons," Phys. Rev. Lett. **98**(12), 123903 (2007).
4. A. V. Kavokin, I. A. Shelykh, and G. Malpuech, "Lossless interface modes at the boundary between two periodic dielectric structures," Phys. Rev. B **72**(23), 233102 (2005).
5. T. Goto, A. V. Dorofeenko, A. M. Merzlikin, A. V. Baryshev, A. P. Vinogradov, M. Inoue, A. A. Lisyansky, and A. B. Granovsky, "Optical tamm states in one-dimensional magnetophotonic structures," Phys. Rev. Lett. **101**(11), 113902 (2008).
6. M. Kaliteevski, I. Iorsh, S. Brand, R. A. Abram, J. M. Chamberlain, A. V. Kavokin, and I. A. Shelykh, "Tamm plasmon-polaritons: Possible electromagnetic states at the interface of a metal and a dielectric Bragg mirror," Phys. Rev. B **76**(16), 165415 (2007).
7. A. Kavokin, I. Shelykh, and G. Malpuech, "Optical tamm states for the fabrication of polariton lasers," Appl. Phys. Lett. **87**(26), 261105 (2005).
8. O. Gazzano, S. de Vasconcellos, K. Gauthron, C. Symonds, J. Bloch, P. Voisin, J. Bellessa, A. Lemaître, and P. Senellart, "Evidence for confined tamm plasmon modes under metallic microdisks and application to the control of spontaneous optical emission," Phys. Rev. Lett. **107**(24), 247402 (2011).
9. C. Symonds, A. Lemaître, E. Homeyer, J. C. Plenet, and J. Bellessa, "Emission of tamm plasmon/exciton polaritons," Appl. Phys. Lett. **95**(15), 151114 (2009).
10. C. H. Xue, H. T. Jiang, and H. Chen, "Nonlinear resonance-enhanced excitation of surface plasmon polaritons," Opt. Lett. **36**(6), 855–857 (2011).
11. H. C. Zhou, G. Yang, K. Wang, H. Long, and P. X. Lu, "Multiple optical tamm states at a metal-dielectric mirror interface," Opt. Lett. **35**(24), 4112–4114 (2010).

12. J. Y. Guo, Y. Sun, Y. W. Zhang, H. Q. Li, H. T. Jiang, and H. Chen, "Experimental investigation of interface states in photonic crystal heterostructures," Phys. Rev. E Stat. Nonlin. Soft Matter Phys. **78**(2), 026607 (2008).
13. A. V. Kavokin and M. A. Kaliteevski, "Excitonic light reflection and absorption in semiconductor microcavities," Solid State Commun. **95**, 859–862 (1995).
14. D. S. Bethune, "Optical harmonic generation and mixing in multilayer media: analysis using optical transfer matrix techniques," J. Opt. Soc. Am. B **6**(5), 910–916 (1989).
15. Z.-Y. Li and L.-L. Lin, "Photonic band structures solved by a plane-wave-based transfer-matrix method," Phys. Rev. E Stat. Nonlin. Soft Matter Phys. **67**(4), 046607 (2003).
16. Z.-Y. Li and K.-M. Ho, "Application of structural symmetries in the plane-wave-based transfer-matrix method for three-dimensional photonic crystal waveguides," Phys. Rev. B **68**(24), 245117 (2003).
17. J. B. Pendry, A. J. Holden, D. J. Robbins, and W. J. Stewart, "Magnetism from conductors and enhanced nonlinear phenomena," IEEE Trans. Microw. Theory Tech. **47**(11), 2075–2084 (1999).
18. N. Liu, H. C. Guo, L. W. Fu, S. Kaiser, H. Schweizer, and H. Giessen, "Three-dimensional photonic metamaterials at optical frequencies," Nat. Mater. **7**(1), 31–37 (2008).
19. C. Rockstuhl, T. Paul, F. Lederer, T. Pertsch, T. Zentgraf, T. P. Meyrath, and H. Giessen, "Transition from thin-film to bulk properties of metamaterials," Phys. Rev. B **77**(3), 035126 (2008).
20. H. T. Jiang, H. Chen, H. Q. Li, Y. W. Zhang, J. Zi, and S. Y. Zhu, "Properties of one-dimensional photonic crystals containing single-negative materials," Phys. Rev. E Stat. Nonlin. Soft Matter Phys. **69**(6 Pt 2), 066607 (2004).
21. N. W. Ashcroft and N. D. Mermin, *Solid State Physics* (Sounders, Philadelphia, 1976).
22. J. Callaway, *Quantum Theory of the Solid State* (Academic Press, Boston, 1991).
23. M. Bayindir, B. Temelkuran, and E. Ozbay, "Tight-binding description of the coupled defect modes in three-dimensional photonic crystals," Phys. Rev. Lett. **84**(10), 2140–2143 (2000).

1. Introduction

Surface waves are common wave phenomena that have been studied in various fields of physics such as acoustics [1], plasma [2] and optics [3]. One type of well known surface waves is the optical Tamm state (OTS) [4, 5], which exists at the interface of photonic crystal (PC) heterostructure. Different from waveguide surface modes and Dyakonov modes, OTSs can remain localized for in-plane wave vector inside the light cone [[4]]. In contrast to a conventional surface plasmon polariton, OTSs can be formed for both the TE and TM polarizations [6]. In addition to the surface of dielectric PC, OTS can also appear at the interface between metal and dielectric Bragg mirror [6].

OTSs can be employed in applications such as the realization of polariton lasers without cavities [7], controlling spontaneous optical emissions [8, 9], enhancing nonlinear resonance [10] and optical switching [11]. So far, there is no way can precisely predict the frequencies of OTSs and this restricts the applications of OTSs. It was proposed that OTSs can be designed by parameter retrieval method [12]. However, such method can no longer be effective for PCs since the scale of the PC is much larger than the wavelength of incident wave. On the other hand, the potential influence of the surface feature of the PC, which should be very relevant to the behavior of surface state, has never been reported.

In this paper, we theoretically investigate the properties of phase shift upon reflection from one-dimensional (1D) PC, including the relationship between the phase shift and the location of the terminating surface in the PC. Base on these properties, we present a convenient and effective method to design OTSs which exist at the interface of PC heterostructure. Furthermore, we point out that dielectric PCs can be equivalent to single-negative (SNG) materials through the properties of their reflection phase. A PC heterostructure supporting OTS is designed and repeated to form a superlattice structure. Our results show that OTSs coupling and zero-effective-phase gap can be observed in such a superlattice structure.

2. OTSs at the interface of PC heterostructure

2.1 Condition for the emergence of OTS

Consider a layered structure composed of two 1D PCs and a sandwich layer, as shown in Fig. 1. The wave will gain a phase change φ when propagating through the sandwich layer from the left (right) interface to the right (left) interface. This structure is analogous to the quantum

well microcavity in quantum mechanics [13] with the sandwich layer being a resonant cavity. The eigenmodes of the structure can be obtained according to the resonant cavity theory. We use $\varphi_{\text{left}}(k_z, \omega)$ and $\varphi_{right}(k_z, \omega)$ to denote the phase shift upon reflection from the left and right interfaces along the x axis, where k is the wave number and ω is the angular frequency. With these definitions, the resonance condition can be written as

$$\varphi_{left}(\omega) + \varphi_{right}(\omega) + 2\varphi = 2m\pi, \tag{1}$$

where $\varphi = nx\omega/c$ is the phase shift of the wave after propagating a distance x in the cavity between the two interfaces. When the resonance condition is satisfied, an OTS corresponding to a transmission mode appears.

If the cavity length x is set to zero, φ becomes zero and Eq. (1) changes to $\varphi_{left}(k_z, \omega) + \varphi_{right}(k_z, \omega) = 2m\pi$. In this case, whether the OTS emerges or not depends solely on the phase changes due to reflections at the cavity boundaries.
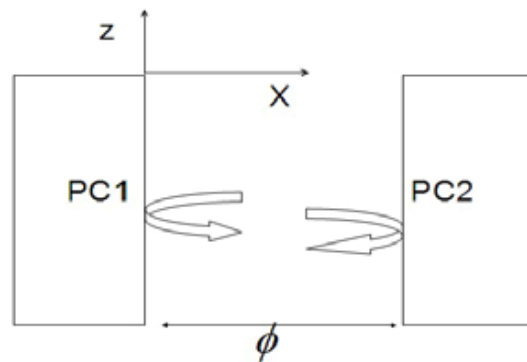
Fig. 1. Schematic illustration of a resonant cavity between two PCs.

2.2 OTSs design based on the reflection phase properties of PC

Firstly, we discuss the phase properties of the reflected wave from the surface of PC. Consider a 1D PC with structure of $(XY)^N$, where X and Y represent SiO$_2$ layer with refractive index of 1.5 and AlAs layer with refractive index of 3, respectively, and N is the number of periods, as shown in Fig. 2. Here we choose $N = 8$. The phase shift of the reflected wave of the PC depends on the refractive index of the adjacent isotropic medium. In the following calculation, we suppose that the isotropic medium is vacuum. The thicknesses of layer X and Y are both 100 nm. In order to study the properties of the reflection phase as a function of the location of the terminating surface within the cell XY, we use the cut parameter t to represent the relative position of the terminating surface in the cell, as shown in Fig. 2. For example, if $t = 1$, the PC terminates with a complete cell; if $t = 0.75$, the cell is terminated in the middle of layer X.
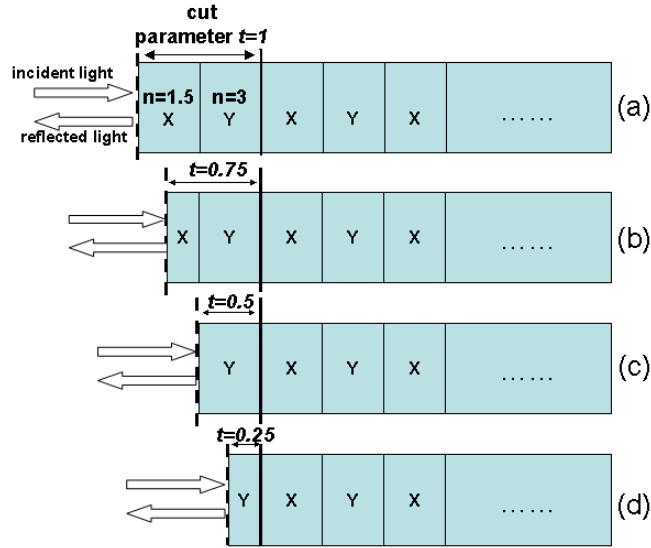
Fig. 2. Variation of the position of the terminating surface plane, marked with a dotted line. (a) *t* = 1, at which the PC terminates with the complete cell at the surface. (b) *t* = 0.75, of which the surface plane is at the middle of media X. (c) *t* = 0.5, the position of the surface plane is at the surface of media Y. (d) *t* = 0.25, the position of the surface plane is at the middle of media Y.

Using the transfer matrix method [14–16], the reflectance and the reflection phase shift φ as functions of wavelength at normal incidence are calculated and shown in Fig. 3(a) and 3(b), respectively. It can be seen from Fig. 3(a) that a Bragg gap appears between 760 nm and 1135 nm. In the stop band, the reflection phase shift changes smoothly across different wavelengths, while the reflection phase shift changes sharply in the pass band regime.
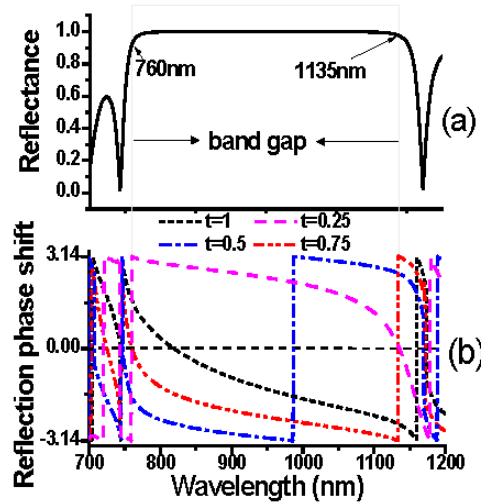
Fig. 3. (a) The reflection spectrum of the PC at normal incidence and (b) the reflection phase spectra for various cut parameter values. The shadow region represents the forbidden gap of PC.

When $t = 0.75$, the reflection phase in the band gap changes from 0 to $-\pi$, which corresponds to the electromagnetic distribution of the PC. Using MIT's MPB software, we obtained the electromagnetic field distribution. Figure 4(a) shows the electromagnetic field

distribution in the PC at the edge of the band gap ($\lambda = 760$ nm) when $t = 0.75$. The electromagnetic field near the surface of the PC is strongest, which means that the superposition of the electric fields of incident light and reflected light is enhanced. Therefore it is deduced that the reflection phase shift should be zero at the surface. Figure 4(b) shows the electromagnetic field distribution at the other edge of the band gap ($\lambda = 1135$ nm). Correspondingly, the superposition of the electric fields leads to a cancellation and the phase shift should be $\pm\pi$.
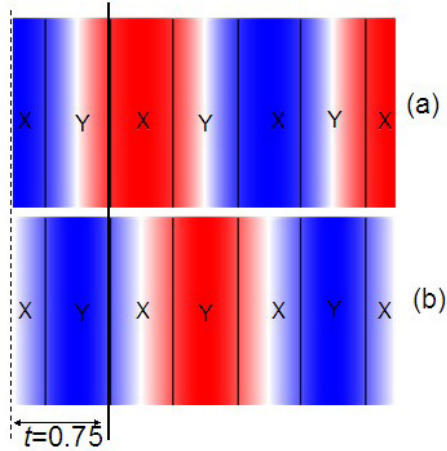
Fig. 4. Electromagnetic field distributions at the two ends of band gap of the PC (c.f. Figure 3) with t = 0.75: (a) wavelength = 760 nm; (b) wavelength = 1135 nm.
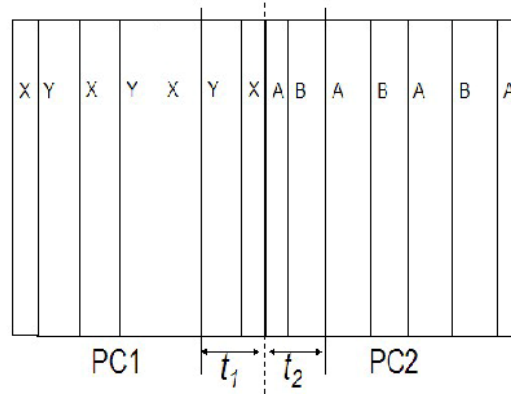
Fig. 5. The structure of a 1D PC heterostructure $[(YX)^N(YX)^{t1}(AB)^{t2}(AB)^M]$

As discussed in section 2.1, the position of the OTS depends on the reflection phase shift, which can be adjusted by the cut parameter t of the PC. Hence, we can design OTS by setting cut parameter t appropriately. Consider a 1D PC heterostructure with the form of $[(YX)^N(YX)^{t1}(AB)^{t2}(AB)^M]$, as shown in Fig. 5, where X and A represent SiO$_2$ layer with the refractive index of 1.5 and the thickness is 100 nm and 80 nm, Y represents AlAs layers with the refractive index of 3 and the thickness is 100 nm, B represents GaAs layers with the refractive index of 3.5 and the thickness is 84nm. Here, the numbers of periods are $N = M = 8$. t_1 and t_2 represent the surface cut parameters for PC cells XY and AB, respectively. Four cases were considered: (a) $t_1 = 0.75$ and $t_2 = 1$; (b) $t_1 = 0.75$ and $t_2 = 0.75$; (c) $t_1 = 0.75$ and $t_2 = 0.5$; and (d) $t_1 = 0.75$ and $t_2 = 0.25$, respectively. The reflection phase shifts φ_{PC1} and φ_{PC2} and the

transmission spectra of the heterostructure are shown in Fig. 6(a) to 6(d), corresponding to t_2 = 1, 0.75, 0.5 and 0.25. It can be seen that a tunneling peak emerges in the overlapping region of the two band gaps when $\varphi_{PC1} + \varphi_{PC2} = 0$, which corresponds to the condition for the emergence of OTS discussed above. For instance, when t_1 = 0.75 and t_2 = 0.75, as the frequency changes across the photonic band gap, both φ_{PC1} and φ_{PC2} change from 0 to π. The condition $\varphi_{PC1} + \varphi_{PC2} = 0$ is impossible to be satisfied in the superposition of the two band gaps. Thus no OTS emerges, as shown clearly in Fig. 6(b). When t_2 = 0.25, the reflection phase shift of PC2 changes from π to 0 across the forbidden gap. An OTS emerges at the wavelength of 944.5 nm, where φ_{PC1} = −2.41 and φ_{PC2} = 2.41, as shown in Fig. 6(d). The inset in Fig. 6(d) shows the distribution of the electric field corresponding to the OTS at 944.5 nm. It can be seen that the field is strongly localized at the interface between the two PCs and attenuates exponentially as getting away from the interface.
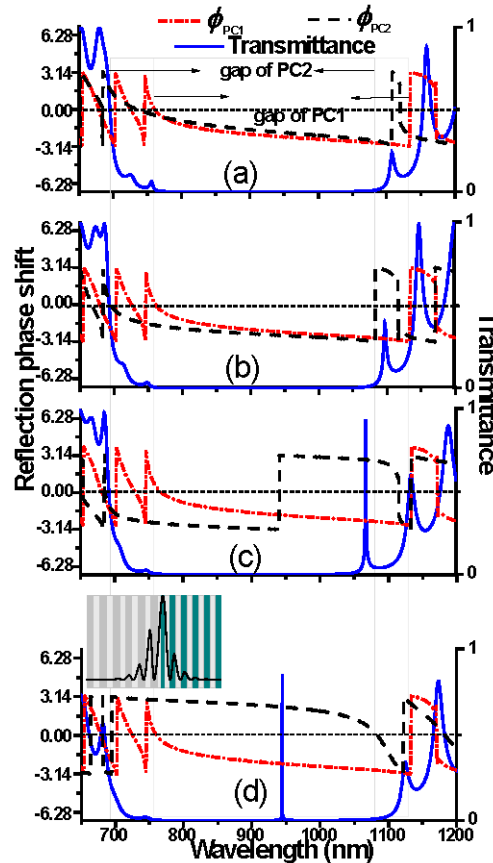
Fig. 6. The reflection phase shifts of PC1 and PC2 and the transmittance of the heterostructure PC1/PC2 shown in Fig. 5, with different cut parameter combinations: (a) t_1 = 0.75 and t_2 = 1; (b) t_1 = 0.75 and t_2 = 0.75; (c) t_1 = 0.75 and t_2 = 0.5; (d) t_1 = 0.75 and t_2 = 0.25. The superposition of the two shadows in each graph is the overlapping of the band gaps of PC1 and PC2. The number of periods for the PCs is $N = M = 8$. The inset in (d) shows the electric field distribution in the heterostructure at 944.5 nm.

3. Transmission bands originate from the coupling of OTSs

3.1 Phase properties and tunneling in SNG materials

In section 2, dielectric PCs were considered as uniform media to discuss the relationship between the reflection phase shifts and the OTSs. Next, we are going to discuss the reflection phase shift of single-negative (epsilon-negative (ENG) or mu-negative (MNG)) materials and analyze the coupling effect of the OTSs.

Here we use Drude–Lorentz model to describe the dispersions of the single-negative materials, that is

$$\varepsilon = 1 + \frac{\omega_p^2 - \omega_{eo}^2}{\omega_{eo}^2 - \omega^2 - i\omega\gamma_e}, \quad \mu = \mu_0 \tag{2}$$

for ENG materials and

$$\varepsilon = \varepsilon_0, \quad \mu = 1 + \frac{F\omega^2}{\omega_o^2 - \omega^2 - i\omega\gamma_m} \tag{3}$$

for MNG materials. Where ω_p, ω_{eo} and ω_o correspond to the electric plasma frequency, the electric resonance frequency and the magnetic resonance frequency, respectively. γ_e and γ_m denote the respective electric and magnetic damping factors that contribute to the absorption and losses. These kinds of dispersions can be realized in well-designed metamaterials [17–19]. For ENG materials, the region of wavelength between $2\pi c/\omega_{eo}$ and $2\pi c/\omega_p$ is a stop band since the permittivity in Eq. (2) is negative. While for MNG materials, the stop band is between $2\pi c/\omega_o$ and $2\pi c/\sqrt{\omega_o^2/(1-F)}$. Here, we choose $\omega_{eo} = 2.093 \times 10^{15}$ Hz, $\omega_p = 4.443 \times 10^{15}$ Hz, $\omega_o = 2.093 \times 10^{15}$ Hz, $F = 0.553$ and $\gamma_e = \gamma_m = 2.0 \times 10^{12}$ Hz.

Figure 7(a) and 7(b) shows the reflection spectra of the SNG materials. Figure 7(c) shows the phase of light reflected from ENG and MNG media and the transmittance of the heterostructure ENG/MNG, respectively. As shown in Fig. 7, in the stop band, the reflection phase shifts of the SNG materials change smoothly as the wavelength changes, while in the pass band the reflection phase shifts change more rapidly, which is analogous with the reflection phase property of dielectric PC. Specially, in the stop band, the reflection phase shift of ENG material changes from 0 to $-\pi$, corresponding to the reflection phase of PC1 and PC2 with the surface cut parameter $t = 0.75$. On the other hand, the reflection phase shift of MNG material changes from π to 0, corresponding to the PC1 and PC2 with the surface cut parameter $t = 0.25$. It can be seen that from Fig. 7(b) that an interface tunneling state appears in the SNG heterostructure [ENG /MNG] when the condition $\varphi_{ENG} + \varphi_{MNG} = 0$ is satisfied. The relative transmittance of interface tunneling state is only approximative 0.45 since the losses in the both ENG and MNG material. Such condition is the same as that for the emergence of OTSs in dielectric PC heterostructure. Therefore, the OTSs at the interface of the PC heterostructure [PC1/PC2] with $t_1 = 0.75$ and $t_2 = 0.25$ is analogous with the tunneling states at the interface of the SNG heterostructure.

If ENG and MNG materials are alternately stacked to construct a periodic structure, then multiple interface tunneling states will emerge and couple each other to form a new transmission band. When specific conditions are satisfied, a zero-effective-phase (zero-φ_{eff}) gap will emerge [19]. These phenomena can also be found in the dielectric PC superlattice structure.
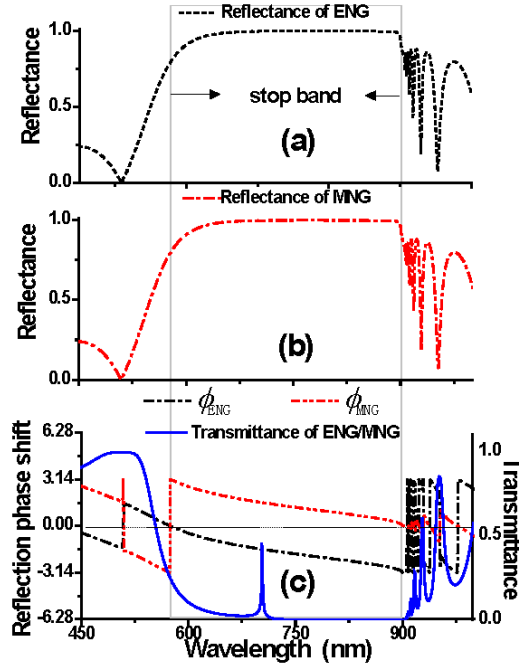
Fig. 7. Reflection spectra of (a) ENG and (b) MNG materials. (c) Reflection phase shifts of both ENG and MNG materials and the transmittance of the heterostructure ENG/MNG. The shadow region represents the common stop band of the SNG materials.

3.2 Coupling of OTSs in dielectric PC superlattice

Consider a sandwich dielectric PC structure [PC1/PC2/PC1], where PC1 and PC2 represent 1D periodic structures $[(XY)^{1-t1}(XY)^{N-1}(XY)^{t1}]$ and $[(AB)^{t2}(AB)^{M-1}(AB)^{1-t2}]$ respectively. Here we take $t_1 = 0.75$, $t_2 = 0.25$, and $N = 6$, $M = 4$. The transmission spectrum of this sandwich structure is showed in Fig. 8(a). We observe that the OTS in the previous case (as shown in Fig. 6(d)) split into two OTSs locate at 930 nm and 963 nm respectively. This splitting is analogous to the splitting in the diatomic molecules, in which the interaction between the two atoms produce a splitting of the degenerate atomic levels into bonding and antibonding orbitals [21]. Here, two interfaces are analogous to two atoms and the length of PC2 is analogous to the distance of two atoms. Therefore, the interaction between the two interfaces of [PC1/PC2/PC1] will split the previous OTS into two new isolated states, as shown in Fig. 8(b). If the structure is extended as [PC1/PC2/PC1/PC2/PC1], the two isolated states will respectively split into two states. If the structure is extended as [PC1/PC2/PC1/PC2/PC1/PC2/PC1], the two isolated states will then respectively split into three states, as shown in Fig. 8(c). These structures can be regard as a crystal composed of numerous diatomic molecules and each diatomic molecule has two isolated states. According to the Tight-Binding (TB) theory [21–23], each isolated states will split and form new bands, respectively. Correspondingly, the band structure of superlattice structure [PC1/PC2]^k shows that two bands emerge in the original band gap, as shown in Fig. 8(d). The gap between the two bands is analogous to the zero-φ_{eff} gap in PCs consisting of ENG and MNG materials.

When the two isolated states are close to each other, the zero-φ_{eff} gap will vanish since the two pass bands couple together. The band structure of PC superlattice structure [PC1/PC2]^k with $N = M = 5$ is shown in Fig. 9. It can be seen that the two pass bands couple together at 945 nm, where the Bloch wave vector is zero. A new pass band form in the range from 928 to 964 nm. As the values of N and M increase, this pass band narrows, as shown in

Fig. 9. According to TB theory, the width of the pass band is in proportion to the overlap integrals of the states. The increasing of the values of M and N means that the interfaces of the PC superlattice leave away from each other, the overlap integrals will diminish and the width of the pass band will narrow.
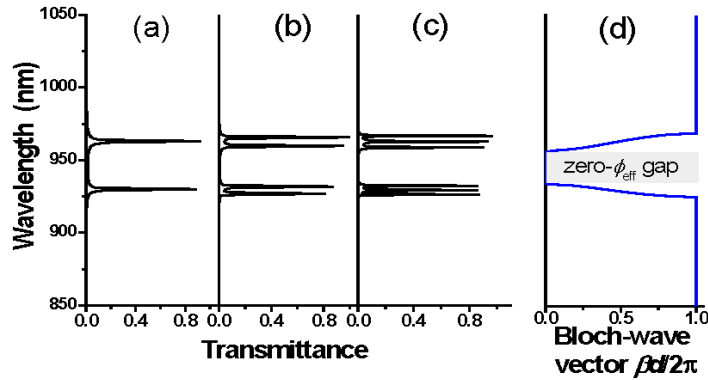
Fig. 8. Transmission spectra of structure (a) [PC1/PC2/PC1], (b) [PC1/PC2/PC1/PC2/PC1], and (c) [PC1/PC2/PC1/PC2/PC1/PC2/PC1]. (d) The band structure of superlattice structure [PC1/PC2]^k with $N = 6$, $M = 4$.
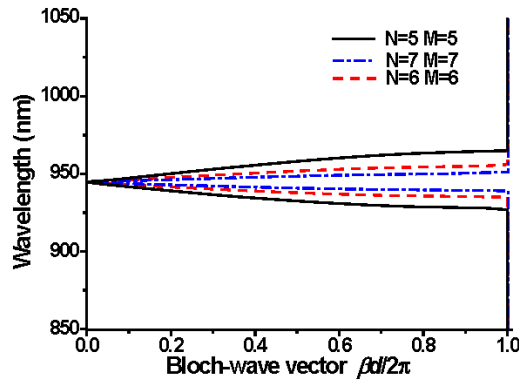
Fig. 9. Band structure of PC superlattice structure [PC1/PC2]^k

4. Conclusion

We demonstrated that the phase shift of the reflected light from a PC depends on the cut parameter of the surface of the PC. By use of such a property, OTSs can be produced and the wavelengths at which the OTSs occur can be tuned at will. We also found that dielectric PCs and SNG materials can be connected through their reflection phase properties. Two kinds of dielectric PCs with different SNG properties are designed and repeated alternately to form a superlattice structure. Multiple OTSs arise in this PC superlattice and these OTSs are coupled with each other to form new transmission bands. A zero-φ_{eff} gap can be observed in such superlattice.

Acknowledgments